MR susceptibility imaging

Jeff Duyn *

Advanced MRI Section, Laboratory of Functional and Molecular Imaging, National Institute of Neurological Disorders and Stroke, National Institutes of Health, Bethesda, MD, USA

ARTICLE INFO

ABSTRACT

This work reviews recent developments in the use of magnetic susceptibility contrast for human MRI, with a focus on the study of brain anatomy. The increase in susceptibility contrast with modern high field scanners has led to novel applications and insights into the sources and mechanism contributing to this contrast in brain tissues. Dedicated experiments have demonstrated that in most of healthy brain, iron and myelin dominate tissue susceptibility variations, although their relative contribution varies substantially. Local variations in these compounds can affect both amplitude and frequency of the MRI signal. In white matter, the myelin sheath introduces an anisotropic susceptibility that has distinct effects on the water compartments inside the axons, between the myelin sheath, and the axonal space, and renders their signals dependent on the angle between the axon and the magnetic field. This offers opportunities to derive tissue properties specific to these cellular compartments.

1. Introduction

One area of MRI that has seen rapid development in recent years is that of contrast based on magnetic susceptibility, which relates to the tendency of tissue to become magnetized by a magnetic field. In large part, this recent development has been catalyzed by the stronger contrast seen with high field systems (up to 9.4 T), which have become available for human MRI. This has resulted in novel ways to exploit and interpret susceptibility contrast, as well as in an improved spatial resolution. As a result, interesting findings have been reported in applications to the study of brain anatomy, which will be the focus of this review.

In biological tissues, susceptibility contrast arises from the subtle field perturbations generated by local variations in magnetic properties. After initially being avoided for its sensitivity to artifacts [1], susceptibility contrast found application to the in vivo study of human brain starting around 1987 at fields as low as 0.15 T [2,3]. Despite the low resolution (several mm) and poor sensitivity to magnetic susceptibility-induced field perturbations (detection limit around 1 ppm), the researchers at this time were able to detect brain abnormalities in a variety of brain pathologies, including stroke, trauma, and tumors. The observed contrast was attributed to paramagnetic effects from blood and its breakdown products.

Since this early work, there has been a steady increase in field strength and with it, an increase in the use of susceptibility contrast. Two important MRI developments followed shortly after the initial applications to brain pathology: bolus tracking based

on an intravascular contrast agent with paramagnetic susceptibility [4], and Blood Oxygen Level Dependent (BOLD) functional MRI [5]. The former method has been extensively used to characterize stroke and tumors in patients by studying perfusion in organs such as brain, prostate, liver, and breast by following the time course of passage of the intravenously injected Gadolinium or Dysprosium chelates through the vasculature [6,7]. BOLD fMRI, based on subtle changes in blood susceptibility in response to changes in neuronal activity, has been used to study brain function and has greatly impacted the field of neuroscience [8]. Both bolus-tracking and BOLD fMRI extended the use of susceptibility contrast from purely anatomical characterization to provide functional information. Notable developments after this have been the use of susceptibility contrast to quantify tissue iron content (for review see [9]) and image the vasculature [10,11], and the use of exogenous, iron oxide based contrast agents for cell tracking [12,13]. Indeed, the exquisite sensitivity of susceptibility weighted imaging enabled the detection of single cells under certain conditions [14].

Twenty-five years since the initial use of susceptibility contrast in human brain, at least forty scanners at 7 T and 9.4 T are in use worldwide, providing unprecedented opportunities for the study of tissue structure and function. In brain, resolutions of around 0.3 mm are possible, with sensitivities to field shifts down to a few ppb (Fig. 1). This is allowing the visualization of fine anatomical detail [15] and subtle pathology [16–19]. In addition, much progress has been made towards the interpretation of magnetic susceptibility contrast, facilitated by the stronger effects seen at high field. Importantly, the major contributing tissue constituents have been catalogued, and methods are being developed to quantify these through the calculation of susceptibility maps [20–22]. In human brain, a very recent finding has been the sensitivity to

* Fax: +1 301 480 1981.
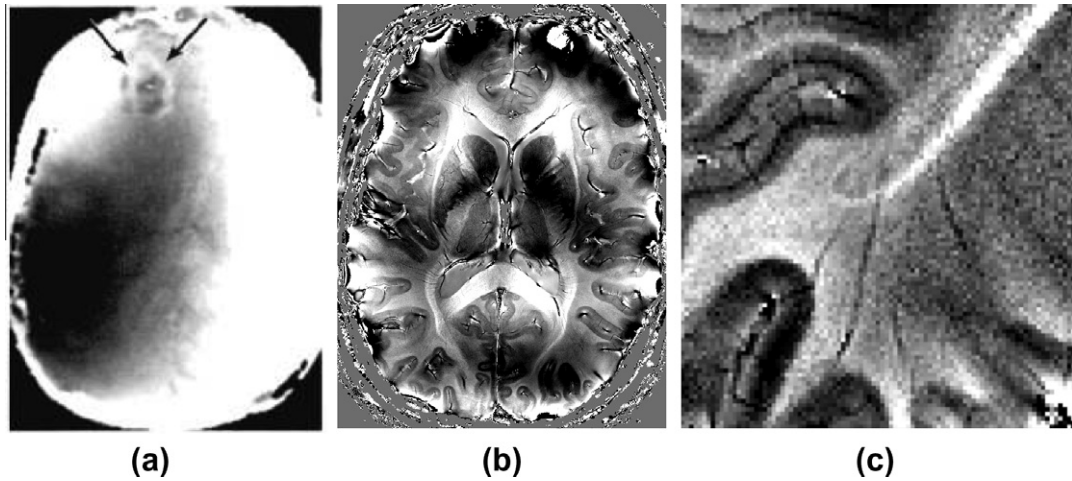*E-mail address:* jhd@helix.nih.gov

Fig. 1. Frequency contrast in the human brain, derived from susceptibility-weighted phase images. Earliest studies date back to the mid-eighties and were performed at a field strength of 0.15 T. (a) is an example of a brain tumor (arrows) which shows a distinct phase shift at its boundary (figure reproduced with permission from Young et al. [2]). Much progress has been made since, using high field (7 T) and array detectors: (b) and (c) show examples of anatomical detail seen in normal brain. Banding and shading effects in (a) and (b) are due to macroscopic susceptibility variations (e.g. air tissue interfaces). Contrast in (b) and (c) is seen between grey and white matter, and between the major fiber bundles and surrounding white matter. Some cortical areas in (c) show laminar contrast.

white matter microstructure and its orientation relative to the MRI magnetic field [23–25], facilitating the identification of the brain's major fiber bundles and the distinction between cellular-scale water compartments [26]. These developments, which will be reviewed in more detail below, are likely to have significant impact on the study of brain anatomy in health and disease.

2. What is magnetic susceptibility?

Magnetic susceptibility can be loosely defined as the degree of magnetization in an object in response to a external magnetic field. As elegantly summarized in [27], magnetization can originate from a number of mechanisms that involve nuclear and electron magnetization, and electron orbits. In brain tissues, the dominant mechanisms are the polarization of unpaired electrons (whose alignment with the applied field is called paramagnetism) and alteration in electron orbits (causing fields opposing the applied field, an effect known as Langevin diamagnetism). Electron orbits are also responsible for the well known nuclear shielding or chemical shift effect in NMR (Fig. 2). Most ions, molecules and compounds naturally present in brain tissue do not have unpaired electrons and therefore exhibit diamagnetism. Notable exceptions are ferritin, hemosiderin, and deoxyhemoglobin, in which the spins of unpaired electrons result in a paramagnetic effect that overwhelms the Langevin diamagnetism. Similarly, exogenous contrast agents such as Gadolinium and Dysprosium chelates, and Iron oxides, have unpaired electrons and are paramagnetic.

An object that is placed in the magnetic field of an MRI system will become magnetized, resulting in a pattern of field changes that depends on object shape and orientation, and generally extends beyond the object's borders (Fig. 3a). These field patterns can be
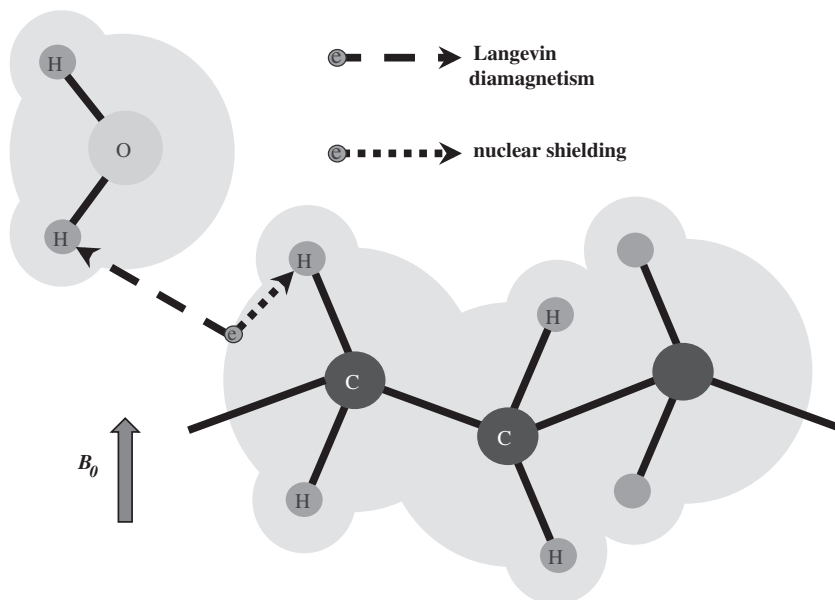

Fig. 2. Main sources of frequency shifts in brain tissues. Orbits of electrons (grey shading) affect the magnetic field sensed at proton nuclei in the same molecule (dotted arrow) and in distant molecules (dashed arrow). These effects are known as nuclear shielding (or chemical shift) and Langevin diamagnetism respectively. In the presence of highly anisotropic molecules (e.g. those with long hydrocarbon chains), both effects can become anisotropic. *Note*: arrows emanating from electron (circle with symbol e) do not represent interaction with electron spin but rather with its orbit, which is dependent on the external magnetic field.

thought of as a convolution of an object's susceptibility distribution with the dipolar field pattern associated with a focal (point-source) susceptibility shift.

In NMR spectroscopy and MRI, these field changes are reflected in a shift of the resonance frequency (Δf). In the example of elongated structures such as infinitely long cylinders, a resonance frequency shift Δf is introduced that has a $\sin^2\theta$ dependence on orientation (Fig. 3b). Resonance frequency shifts have two major effects: first, they offer an opportunity to extract information about the magnetic properties of the object from the NMR signal; second, they may lead to undesired effects such as signal loss, spectral peak

(a)

anisotropic field shift

$$\Delta f_\theta = \Delta f_{\theta=0} - \frac{\gamma}{2\pi} \cdot B_0 \cdot \chi \cdot 0.5 \cdot \sin^2\theta$$

(b)

Fig. 3. Objects placed in magnetic field generate a pattern of field shifts that depends on object shape and orientation (a). Elongated objects such as infinite cylinders, experience a $\sin^2$ dependency of the internal field shift with θ, representing the angle between fiber long axis and B_0, the MRI main magnetic field (b).

shifting and line broadening, and image distortions. The goal of susceptibility imaging with MRI is to exploit the former, while minimizing or accounting for effects of the latter.

In the human body, this pattern of susceptibility-induced field changes can be highly complex, as the underlying magnetic properties vary over the atomic (sub-nanometer) scale. Considering the human body has on the order of 10^{28} atoms, it becomes clear that fully resolving its magnetic structure is well beyond the capabilities of MRI. Nevertheless, as will be seen in the following, anatomically relevant macroscopic (supra-voxel scale) and microscopic (sub-voxel scale) information can be extracted with dedicated MRI experiments and analysis techniques.

3. Sensitization to magnetic susceptibility

While most MRI techniques have some sensitivity to signal loss and resonance frequency shifts resulting from magnetic susceptibility variations in the object, this sensitivity is particularly high for gradient echo (GRE) or free induction decay (FID) type acquisitions [28]. After signal excitation, this technique (Fig. 4) allows the signal to decay freely under the influence of a combination of T_2 (spin–spin coupling) and the spin coherence loss resulting from the susceptibility-induced field variations. The latter is generally indicated by T_2' (implicitly assuming a single exponential signal decay) and the combined effects of T_2 and T_2' are indicated by T_2^* ($1/T_2^* = 1/T_2 + 1/T_2'$).

The simplest susceptibility-weighted technique samples the FID signal at a single time point (i.e. echo time TE) along the decay curve with a GRE readout (Fig. 4a); both amplitude and phase of this signal can then be extracted and interpreted. After correction of phase jumps and large scale effects from tissue/air interfaces and coil phase [15], a reasonably accurate estimate of the local mean frequency can be made by dividing the phase by echo time (this assumes phase equals 0 at TE = 0). Alternatively, two time points (two TE's) can be measured and the instantaneous local frequency can be determined from the phase difference divided by the TE difference. Either approach is exquisitely sensitive, and can under favorable conditions (high field, optimized TE) lead to a precision of less than 1 ppb [15]. In the susceptibility literature, one area of confusion (to which the author of this article has contributed) has been inconsistent use of the sign of the frequency shift: it is recommended to follow the standard convention in which frequency increases (i.e. paramagnetic shifts) are given positive numbers (and bright image intensity).

As mentioned above, the signal level in the magnitude image of the FID technique is affected by both spin density and T_2^* effects. These can be separated by comparing the signal in images obtained at two TE's, providing a quantitative measure of T_2^*. Unfortunately, interpretation of these images may be difficult because T_2^* includes T_2 effects that may not reflect tissue magnetic susceptibility.

In recent years, it has become increasingly clear that in many tissues, T_2^* decay may not be mono-exponential [29–32], and single T_2^* or frequency values may incompletely or even incorrectly characterize the underlying tissue properties. A major contributor to these more complex relaxation characteristics may be restricted diffusion or water compartmentalization to e.g. intra- and extracellular or intra- and extravascular spaces (see below). Thus, it may be beneficial to more completely sample the FID decay curve, for example by spectroscopic imaging techniques such as MESSI and HiSS [33,34], which have been used previously to look at the effects of tissue compartmentalization on water relaxation characteristics. A practical implementation of this is the acquisition of multiple GRE signals with a single excitation (Fig. 4b), which can then be analyzed to more fully characterize and quantify the underlying tissue properties.
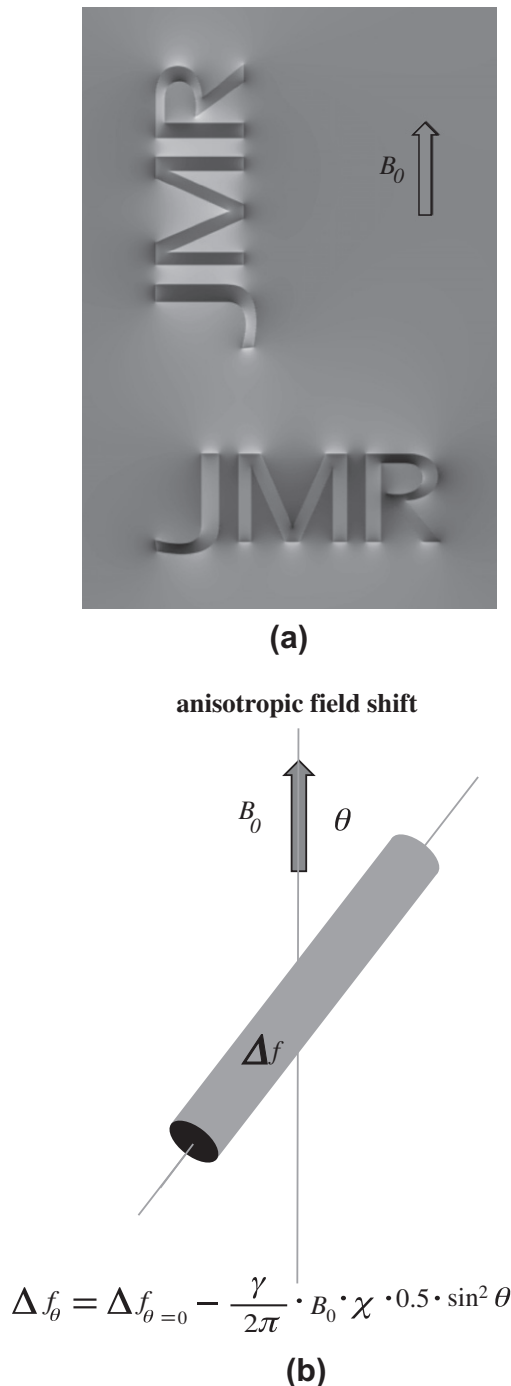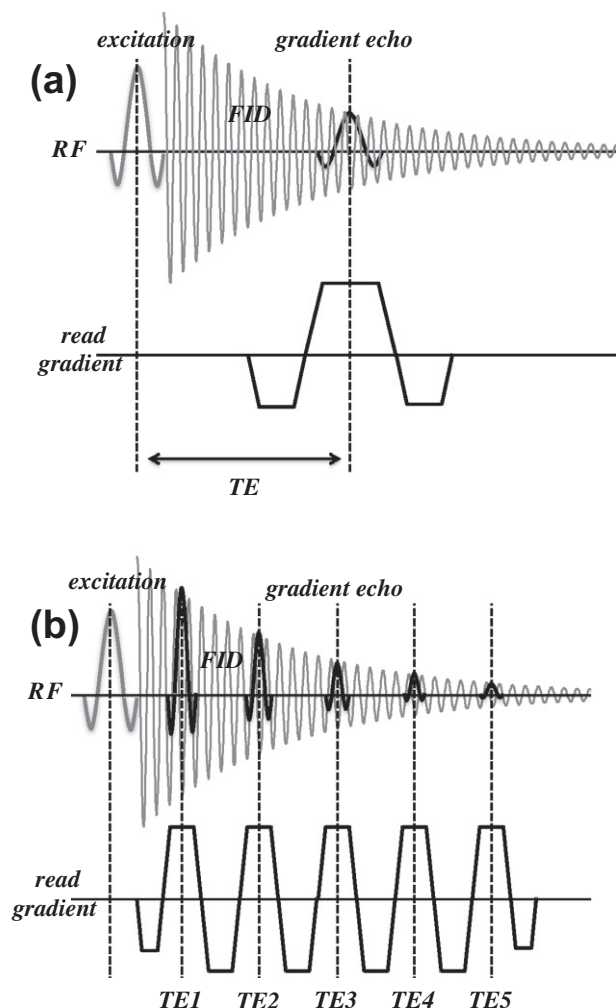
Fig. 4. (a) Basic MRI pulse sequence used for susceptibility-weighted MRI. Only RF and readout gradient are shown. After signal excitation, the FID signal is sampled with a gradient echo centered at the echo time (TE). (b) Modified pulse sequence to more completely sample the FID. Multiple echoes are sampled over a range of TE's, allowing analysis of the decay characteristics and extraction of quantitative parameters.

4. Extraction of quantitative measures of susceptibility

Although the title of this review "MR susceptibility imaging" suggests a rather specific technique, the actual information extracted from susceptibility-weighted signals can vary substantially. In addition to generating magnitude T_2^*-weighted, T_2^*, relaxation rate ($R_2^* = 1/T_2^*$), phase and frequency images, it is possible to combine T_2^*-weighted and phase/frequency data into so-called SWI's (Susceptibility Weighted Images [11]). SWI's provide a single measure for a voxel's frequency shift and distribution, an approach that has been found particularly useful for highlighting vascular structures [35]. A drawback of this method is that it may not allow the extraction of quantitative information in a straightforward manner.

An advantage of extracting parametric information such as T_2^*, R_2^* and frequency is that it eliminates or reduces confounds such as spin density, T_1, and RF coil sensitivity variations. Thus, this information may provide a more robust and quantitative measure of the underlying tissue properties. For example, an important application of R_2^* images has been the quantification of tissue iron content [9]. In fact, R_2^* dependence on iron content has been shown to be approximately linear [36].

Although the role of iron for brain development, homeostasis and function remains poorly understood, iron dysregulation has been recognized as a potential factor in a number of diseases [37,38]. T_2^* contrast may provide a marker of tissue iron content with a sensitivity superior to T_1 and T_2, in particular at high field. A drawback that all these contrast share is that they may be rather sensitive to the microscopic susceptibility distribution as well as effect of diffusion in the associated local field gradients [39,40]. Additionally, R_2^* changes may be non-local due to the dipolar phase patterns associated with a focal susceptibility shift. Such dipolar patterns may result in magnetic field (and R_2^*) changes outside an area of altered susceptibility. This non-local effect on R_2^* can be reduced by scanning at high spatial resolution.

Frequency information derived from susceptibility imaging may be quit valuable as it not only may allow extraction of quantitative tissue information, but also is sensitive to the direction of the local susceptibility shift, and therefore may allow distinguishing between diamagnetic or paramagnetic effects. In this regard, frequency information is complementary to R_2^* information derived from magnitude images. In human brain, frequency has been used in a number of applications, including the estimation of vascular oxygenation [41–43], the distinction between hemorrhages and calcifications [44,45], and the estimation of tissue iron content [46]. A drawback of frequency information is that it only indirectly reflects an area's susceptibility shift as the associated field effects are generally non-local and depend on the area's shape and orientation. This can be overcome by conversion of frequency information into susceptibility maps.

Over the last few years, various methods have been developed to reconstruct tissue susceptibility distributions from frequency maps [20–22,47–50]. These susceptibility mapping methods would overcome some of the problems of frequency maps and resolve dependencies on shape and orientation. Most methods apply the Fourier filtering technique to calculate susceptibility from frequency [51,52], which in effect is a deconvolution of the dipolar phase patterns associated with point source susceptibility perturbations. Unfortunately, susceptibility methods are sensitive to noise amplification and streaking artifacts [20], which can be mitigated by regularization [20,53], or the acquisition of frequency data at multiple head orientations [54]. Recent methods have shown excellent results relying only on single orientation data by incorporating a priori information [49,55] or constraints on the smoothness of the frequency data [50].

A caveat with all current susceptibility mapping methods is the implicit assumption that frequency maps closely reflect the underlying field distribution, which is not always the case (e.g. in white matter, see below). Future refinements undoubtedly will address this issue.

5. Contributors to magnetic susceptibility contrast in brain

Which compounds or molecules cause magnetic susceptibility variations in the brain? Among the main candidates are iron in deoxyhemoglobin and storage proteins, and myelin, and their contribution to image contrast has been shown to vary strongly across brain regions. Here we briefly review the major recent findings regarding the effect of iron and myelin in grey matter (GM) and white matter (WM) of the brain.

A salient finding with susceptibility imaging has been the conspicuity of vascular structures, in particular at high field [56]. This contrast, primarily seen in the venous vasculature, can be attributed to deoxyhemoglobin, and forms the basis of venography techniques such as SWI [11]. It is also responsible for the contrast seen in highly vascular regions associated with tumor growth [35]. Extravasation of blood may result in the breakdown of hemoglobin

and sequestration of iron in hemosiderin and ferritin, which are responsible for the contrast seen in hemorrhagic stroke and traumatic brain injury [35]. In functional brain studies, analysis of the signal decay and frequency shifts associated with deoxyhemoglobin in the vasculature may allow the measurement of blood oxygenation [41,57].

The basal ganglia generally show substantial signal loss in T_2 and T_2^* weighted magnitude images [58,59], and a frequency shift [46], and these effects can be attributed to the high iron content of these regions [9,58]. In fact, there is a high linear correlation between R_2^* and iron content (in ppm) in these regions with proportionality constant that increases linearly with field by about 0.01 Hz/T/ppm [36].

Within cortical gray matter, a laminar variation in frequency and R_2^* has been observed [15,60] and this has been attributed to iron in ferritin [60]. Deoxyhemoglobin does not substantially contribute to this contrast [61], despite the substantial laminar differences in vascularization [62].

An early finding with susceptibility imaging has been the substantial frequency difference between GM and WM [63], despite the small difference in their iron content [64]. It has been proposed that this contrast may be dominated by differences in myelin content [15,46], and recent animal and human studies support this notion [65–68].

One of the most intriguing findings with susceptibility imaging is that of substantial frequency and amplitude variations in WM, in particular around the major fiber bundles in central brain regions [15,69]. This despite the fact that central WM, in contrast to subcortical U-fibers, has relatively low iron content that does not vary substantially between bundles [69,70]. On the other hand, myelin density does vary substantially between bundles and therefore may be a major cause for the relatively large signal loss in the more heavily myelinated fiber bundles seen in T_2 and T_2^* weighted MRI [69,70]. However the magnitude of the frequency difference between these bundles (in excess of 5 Hz at 7 T) appears to be too large to be fully explained by myelin density.

Several recent imaging studies in human brain have observed a strong dependence of frequency and amplitude on fiber bundle orientation relative to the magnetic field [23,71–74], mimicking earlier findings in the muscle fibers of the heart [75]. In the brain's most heavily myelinated fiber bundles, this can lead to an up to 50% increase in R_2^* between fibers parallel and perpendicular with the field [76]. Two distinct mechanisms have been proposed to explain this orientation dependence: anisotropic cellular structure and anisotropic susceptibility [24,25,77]. Each will be discussed in the following sections.

6. Effects of tissue microstructure and orientation

It has been long recognized that transverse relaxation (i.e. T_2 and T_2^* relaxation) may be affected by the microscopic distribution of susceptibility perturbers, i.e. the magnetic microstructure of the object. This distribution affects the associated field patterns, and together with diffusion effects, the phase dispersion across the spin population [29,39,40]. In addition, T_2^* may become orientation dependent when the susceptibility distribution is anisotropic. For example, for elongated susceptibility perturbers, a sine^2 dependence of R_2^* on orientation θ is predicted [29].

Does the microscopic distribution of susceptibility perturbers also affect the average local frequency? This would be expected based on the notion that a water compartment's shape affects its mean (bulk) frequency shift [78]. Several studies have suggested that this may be the case [77,79]. If tissue contains an anisotropic
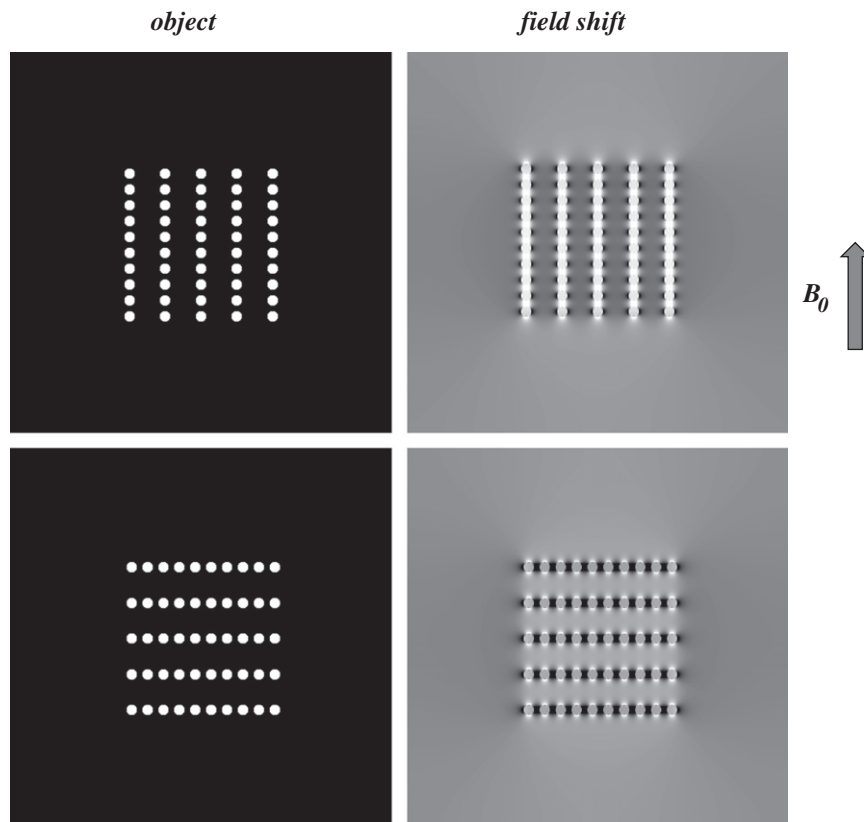

Fig. 5. Simulated dependence of field shift on object microstructure. Water molecules preferentially sample the space between the susceptibility perturbers (white), leading to a biased sampling of the magnetic field pattern and a bias in the resulting mean (voxel averaged) frequency. This bias is dependent on the distribution of perturbers, and on the orientation of the distribution pattern.

distribution of susceptibility perturbers, the water protons will also be anisotropically distributed, and therefore sample the field distribution in a biased manner that affects the mean frequency in an orientation dependent way (Fig. 5).

This has for example been observed for extra-myocellular lipid in muscle tissue, which is present in elongated clusters [79]. Similarly, in WM, myelin is distributed around axons as a hollow cylinder, leaving elongated water compartments to sample the field distribution. As is the case for lipid in muscle, this may lead to orientation dependent frequency shifts. For such elongated compartments in water and muscle, a $sine^2$ dependence of frequency on orientation θ is introduced [77–79], similar to that seen for R_2' [29]. This effect needs to be taken into account when reconstructing susceptibility maps from frequency data.

7. Anisotropic susceptibility

Frequency and R_2^* in WM are not only be affected by structure at the cellular scale, but also by structure at the molecular scale. The latter introduces an orientation dependent disturbance in electron orbit, which may manifests itself as the phenomenon of chemical shift anisotropy that is particularly apparent in solid state NMR. The same mechanism is also expected to result in anisotropic susceptibility. In fact, anisotropic susceptibility has been observed in biological structures of various sizes including helical proteins [80], lipid bilayers [81], retinal rods [82], and muscle fibers [83].

Direct evidence for an anisotropic susceptibility in WM has come from a study of post mortem tissue, which compared the magnetic field effect from an excised, intact WM fiber bundle with that of a modified bundle of which two cubical segments were cut out and rotated 90°, relative to the magnetic field [24]. This manipulation altered the microstructural arrangement of fibers, but not the macroscopic shape. Macroscopic field changes were observed outside the fiber bundle, despite that absence of changes in macroscopic shape. This indicated an anisotropic effect of microstructure on WM
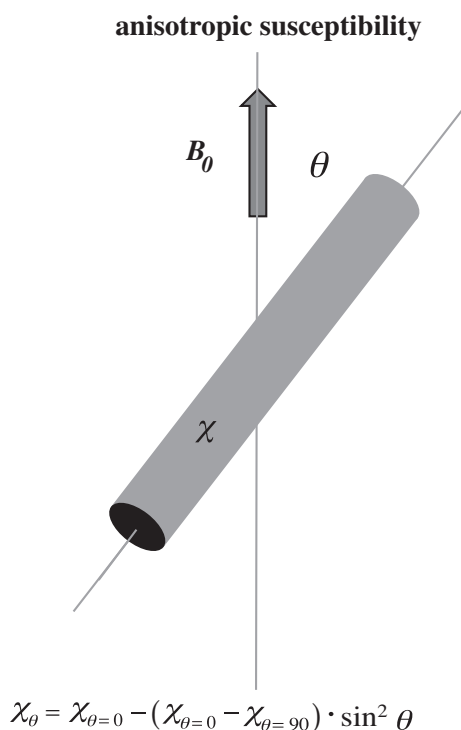

anisotropic susceptibility

$$\chi_\theta = \chi_{\theta=0} - (\chi_{\theta=0} - \chi_{\theta=90}) \cdot \sin^2 \theta$$

Fig. 6. Long cylindrical objects with highly organized microstructure (such as myelinated axons) may exhibit anisotropic susceptibility that has a $\sin^2\theta$ dependence on their angle with the magnetic field.

susceptibility, explained by an anisotropic susceptibility of the myelin sheath [24]. In addition, indirect evidence for anisotropic susceptibility has come from the analysis of MRI of rat brain at various orientations with the magnetic field [25]. This anisotropy results in a white matter susceptibility that has a $\sin^2\theta$ dependence on fiber orientation (Fig. 6). By proper modeling of the macroscopic field variations associated with anisotropic susceptibility, the anisotropy of the brain's major fiber bundles has been quantified [25,84]. A caveat with these techniques is that they do not take into account the effects of microstructure and the associated compartmental bias (see previous section) on the local frequency.

What are the molecular origins of anisotropic susceptibility of WM? A likely source is the alkyl chains of the phospholipids which make up about 25% of the myelin-water system surrounding axons [85,86] and are positioned in a highly organized fashion in the myelin sheath (Fig. 7), the average orientation (relative to the field) of which is dependent on axon and fiber bundle direction. In fact, an early study has shown that alkyl chains exhibit a diamagnetic anisotropy that is about 10% of their overall susceptibility [87]. Assuming the latter to be roughly 10 ppm (similar to 9.04 ppm of water), and taking into account the orientational averaging around the cylindrical shape of the myelin around the axon, as well as the about 20% fraction of hydrated myelin in WM, this leads to an estimate of about 0.027 ppm for the anisotropy of WM. This value is consistent with the range of 0.01 and 0.028 for estimates from in vivo and post-mortem experiments [24,88]. It is also consistent with field modeling studies of tissue compartment specific frequency shifts discussed below.

8. Multicomponent relaxation

As indicated above, the presence of multiple, distinct water environments in a tissue voxel may result in signal decay that is more complex than single-exponential. In fact, multi-exponential T_2 decay has been observed in WM, and interpreted as arising from distinct contributions from water trapped between myelin sheaths on one hand, and axonal and interstitial (between axons) on the other [89,90]. Similar effects have been observed in peripheral nerve [91]. The different association of water with macromolecules in these pools and the limited diffusion and exchange between them (on the T_2 timescale of tens of milliseconds), leads to at least two relaxation components with different T_2's, the shortest of which can be assigned to myelin water [92]. This distinction allows selective imaging of the myelin water pool, which may have important applications to the study of brain myelination and demyelinating diseases such as multiple sclerosis [93].

Interestingly, multi-component relaxation in WM has also been observed with T_2^*-weighted techniques [31,32,94]. Multi-component fitting demonstrates the presence of three major signal components with distinct T_2^* values and frequencies, suggesting three water pools that are differentially affected by magnetic susceptibility effects [26,32]. Furthermore, relaxation differences were dependent on fiber orientation, with the largest differences observed for fibers perpendicular to the magnetic field [26].

Can these three components be assigned to myelin water, axonal water, and interstitial water? There are currently two pieces of evidence that suggest this is indeed justified. First, like with T_2 relaxation, the myelinic origin of the shortest component (with highest frequency) can be established with pulsed magnetization transfer experiments [26,92]. Second, experimental signal decay curves can be accurately predicted from field modeling that assumes the tissues microscopic field variations to be dominated by an anisotropic diamagnetic susceptibility of the myelin sheath with realistic values (a susceptibility difference of about 0.2 ppm between sheath orientations parallel and perpendicular to the field
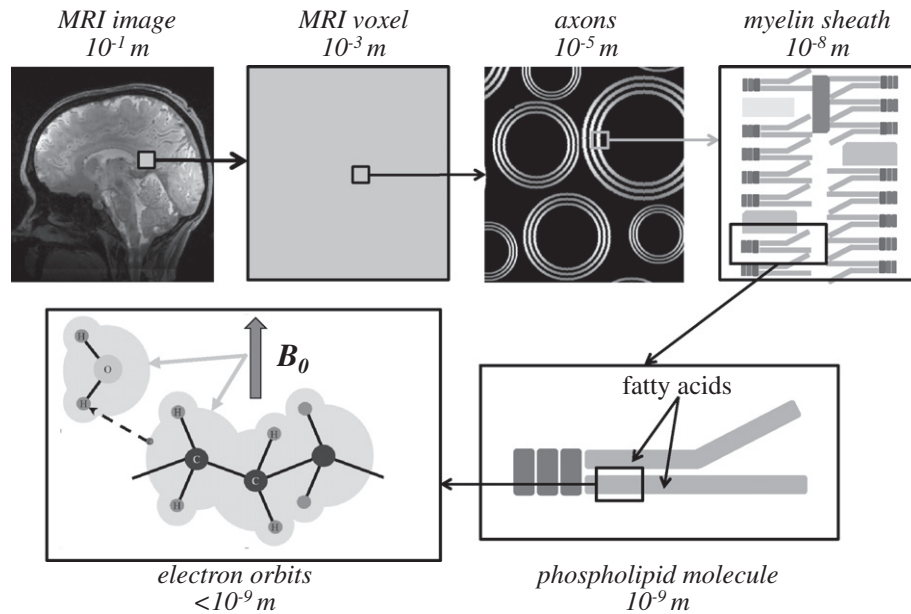
Fig. 7. Magnetic susceptibility effects occur at various spatial scales, ranging from the overall size of the object to the molecular and atomic scale. The diamagnetic susceptibility characteristic for brain tissues primarily arises from the effect of the applied magnetic field on electron orbits (bottom left panel). In white matter fibers with highly organized molecular structure, anisotropic susceptibility can arise from the field angle dependent inter-molecular interaction between electron orbits and water protons (dashed arrow). A candidate for this interaction is the orderly arranged phospholipids that make up the myelin sheath.

[26]). Thus, it may be possible to separately image the three different water pools based on their T_2^* relaxation characteristics. This also suggests that both the microscopic water compartmentalization and anisotropic susceptibility affect the observed amplitude and frequency in susceptibility-weighted MRI, and that one needs to be careful calculating susceptibility maps from frequency data as the instantaneous frequency can be (1) TE dependent and (2) different from frequency shifts that would be observed for magnetically uniform tissue.

9. Exogenous contrast agents

MRI tissue contrast can be substantially altered by the intravascular injection of contrast agents. Paramagnetic contrast agents such as Dysprosium and Gadolinium (Gd) chelates have found widespread use for vascular MRI because of their shortening effect on T_1, that leads to enhancement of the vascular signal in T_1-weighted MRI. Depending on their spatial distribution, these exogenous agents may also provide useful magnetic susceptibility contrast. For example, in cortical GM, where capillary spacing exceeds the typical diffusion distance, injection of a bolus of Gd (which, in the brain, remains intravascular) will affect T_2 and T_2^* [39,40]. Tracking of the bolus passage through the vasculature using dynamic MRI (with either T_2^* or T_2 weighting), allows one to analyze vascular characteristics and estimate cerebral blood flow and volume [4]. Similarly, nano- to micrometer sized superparamagnetic iron oxide (SPIO) particles can be injected and their effect on T_2^* can be measured before and at some delay after injection to estimate cerebral blood volume [95].

It is also possible to use SPIO particles to track the position of specific cells in the body. For example, SPIO particles injected in the vasculature are taken up by immune cells, which allows them to be tracked based on their effect on T_2^* (for reviews see [13,96]). Alternatively, cells can be loaded with SPIO particles outside the body, and followed with susceptibility-weighted MRI after subsequent reinjection. Examples are tracking of immune, tumor, and neural stem cells (for reviews see [12,96]). Tracking of a single cell has been demonstrated by using micron-size particles [14].

An interesting recent development is the precise control of a particle's relaxation properties by micro-fabrication. Micron-size particles can be designed and fabricated that are strongly paramagnetic and produce large, locally homogeneous field shifts. This facilitates their identification by MRI, and may further allow contrast amplification through diffusion-mediated MT effects [97]. Although these particles have not been used in vivo, phantom experiments have shown promising results [97,98].

10. Summary and outlook

The magnetic properties of brain tissue, relevant to susceptibility imaging based on MRI, are dominated by iron, myelin and deoxyhemoglobin, whose distribution in the brain is highly heterogeneous at various spatial scales. These scales span from the few nanometers diameter of ferritin particles and myelin bilayers, to the millimeters size dimension of structures such as the venous vasculature, the cortical thickness, the major fiber bundles, and the basal ganglia. The resulting heterogeneity in the magnetic field is reflected in the amplitude and phase of susceptibility-weighted images.

Field heterogeneity at the microscopic scale leads to an increase in R_2^* and under certain conditions may lead to multi-component relaxation. For example, the anisotropic microscopic structure of WM, and its anisotropic susceptibility, lead to three relaxation components with different R_2^* values and frequencies, most of which are orientation dependent. These components can be attributed to the different water compartments that each sample a specific part of the field distribution. Quantification of these compounds may be possible and allow study of a cellular compartment-specific impact of disease.

Field heterogeneity at the macroscopic scale depends in a convoluted manner on the underlying susceptibility distribution. The latter can be extracted with susceptibility mapping methods, provided any microstructural effects on the frequency are taken into account. This is currently an active area of research. Susceptibility maps are expected to find application to the study of pathologies such as microbleeds and traumatic brain injury, stroke, tumors,

multiple sclerosis, and hemorrhages. They overcome the limitations of phase/frequency maps in distinguishing between effects of diamagnetic compounds (calcifications) and paramagnetic compounds (e.g. increases in iron or deoxyhemoglobin).

Interesting potential applications of susceptibility contrast are fiber mapping [25,74] and tractography [99]. These applications exploit the orientation dependence introduced by the anisotropic structure and susceptibility of WM. Unfortunately they require object rotation in the magnetic field, which is a significant limitation for human studies.

One aspect of susceptibility contrast that deserves further investigation is the effect of diffusion through susceptibility-induced field gradients on T_2 decay in tissues such as WM, an effect to which most spin echo experiments used to generate T_2 contrast are sensitive [100]. Given that the field gradients associated with anisotropic structures are orientation dependent, one would expect some orientation dependence of T_2 in WM. Such susceptibility-induced orientation dependence has been observed with intravascular contrast agents in the anisotropic capillary bed of the heart wall [101]. It may be worth investigating whether this effect is present in brain tissues (without contrast agent) at high field, at which endogenous susceptibility effects are much stronger. Note that the above mechanism for T_2 orientation dependence is different than that underlying the orientation dependent T_2 that has been observed in skeletal muscle [102], peripheral nerve [103], and cartilage [104], which has been attributed to dipole–dipole interactions of oriented water molecules. It has been suggested that the latter effect may not be observable in brain tissues [105].

Study of the distribution of iron in the brain may increase insight into its role for normal brain development function and pathology. Iron is a precursor for the generation of myelin and may be present in increased concentration (in the form of ferritin) when needed for initial myelination of axons during development [106]. It also may continue to be present preferentially at strategic locations near axons that have substantial turnover of myelin, e.g. near the axon terminals, where it may serve as source for iron transport along the axon [107]. Unresolved findings in this regard are the high levels of iron in location like the subcortical U-fibers [58,60], in the line of Gennari in visual cortex [60], and the generally punctuated distribution of iron in subcortical WM [106].

Many of the recent findings in this field have greatly benefited from the increased contrast to noise at 7 T compared to lower field strengths. The continued move to even higher field (9.4 T [108] and above) is expected to further increase susceptibility contrast [109] and it is expected that this will help answering remaining questions about contrast origins, and lead to new findings and applications.

Acknowledgment

References

[1] K.M. Ludeke, P. Roschmann, R. Tischler, Susceptibility artefacts in NMR imaging, Magn. Reson. Imaging 3 (1985) 329–343.
[2] I.R. Young, S. Khenia, D.G. Thomas, C.H. Davis, D.G. Gadian, I.J. Cox, B.D. Ross, G.M. Bydder, Clinical magnetic susceptibility mapping of the brain, J. Comput. Assist. Tomogr. 11 (1987) 2–6.
[3] I.R. Young, G.M. Bydder, S. Khenia, A.G. Collins, Assessment of phase and amplitude effects due to susceptibility variations in MR imaging of the brain, J. Comput. Assist. Tomogr. 13 (1989) 490–494.
[4] A. Villringer, B.R. Rosen, J.W. Belliveau, J.L. Ackerman, R.B. Lauffer, R.B. Buxton, Y.S. Chao, V.J. Wedeen, T.J. Brady, Dynamic imaging with lanthanide chelates in normal brain: contrast due to magnetic susceptibility effects, Magn. Reson. Med. 6 (1988) 164–174.
[5] S. Ogawa, D.W. Tank, R. Menon, J.M. Ellermann, S.G. Kim, H. Merkle, K. Ugurbil, Intrinsic signal changes accompanying sensory stimulation: functional brain mapping with magnetic resonance imaging, Proc. Natl. Acad. Sci. USA 89 (1992) 5951–5955.
[6] A.J. Yoo, B. Pulli, R.G. Gonzalez, Imaging-based treatment selection for intravenous and intra-arterial stroke therapies: a comprehensive review, Expert Rev. Cardiovasc. Ther 9 (2011) 857–876.
[7] J. Missbach-Guentner, J. Hunia, F. Alves, Tumor blood vessel visualization, Int. J. Dev. Biol. 55 (2011) 535–546.
[8] R.A. Poldrack, The role of fMRI in cognitive neuroscience: where do we stand?, Curr Opin. Neurobiol. 18 (2008) 223–226.
[9] E.M. Haacke, N.Y. Cheng, M.J. House, Q. Liu, J. Neelavalli, R.J. Ogg, A. Khan, M. Ayaz, W. Kirsch, A. Obenaus, Imaging iron stores in the brain using magnetic resonance imaging, Magn. Reson. Imaging 23 (2005) 1–25.
[10] J.R. Reichenbach, R. Venkatesan, D.J. Schillinger, D.K. Kido, E.M. Haacke, Small vessels in the human brain: MR venography with deoxyhemoglobin as an intrinsic contrast agent, Radiology 204 (1997) 272–277.
[11] E.M. Haacke, Y. Xu, Y.C. Cheng, J.R. Reichenbach, Susceptibility weighted imaging (SWI), Magn. Reson. Med. 52 (2004) 612–618.
[12] S.M.C. Berman, P. Walczak, J.W.M. Bulte, Tracking stem cells using magnetic nanoparticles, Wires Nanomed. Nanobiotechnol. 3 (2011) 343–355.
[13] G. Stoll, M. Bendszus, New approaches to neuroimaging of central nervous system inflammation, Curr. Opin. Neurol. 23 (2010) 282–286.
[14] E.M. Shapiro, K. Sharer, S. Skrtic, A.P. Koretsky, In vivo detection of single cells by MRI, Magn. Reson. Med. 55 (2006) 242–249.
[15] J.H. Duyn, P. van Gelderen, T.Q. Li, J.A. de Zwart, A.P. Koretsky, M. Fukunaga, High-field MRI of brain cortical substructure based on signal phase, Proc. Natl. Acad. Sci. USA 104 (2007) 11796–11801.
[16] C. Mainero, T. Benner, A. Radding, A. van der Kouwe, R. Jensen, B.R. Rosen, R.P. Kinkel, In vivo imaging of cortical pathology in multiple sclerosis using ultra-high field MRI, Neurology 73 (2009) 941–948.
[17] J.Y. Kwan, S.Y. Jeong, P. Van Gelderen, H.X. Deng, M.M. Quezado, L.E. Danielian, J.A. Butman, L. Chen, E. Bayat, J. Russell, T. Siddique, J.H. Duyn, T.A. Rouault, M.K. Floeter, Iron accumulation in deep cortical layers accounts for MRI signal abnormalities in ALS: correlating 7 Tesla MRI and pathology, PLoS One 7 (2012) e35241.
[18] K.E. Hammond, M. Metcalf, L. Carvajal, D.T. Okuda, R. Srinivasan, D. Vigneron, S.J. Nelson, D. Pelletier, Quantitative in vivo magnetic resonance imaging of multiple sclerosis at 7 Tesla with sensitivity to iron, Ann. Neurol. 64 (2008) 707–713.
[19] N. Madan, P.E. Grant, New directions in clinical imaging of cortical dysplasias, Epilepsia 50 (Suppl. 9) (2009) 9–18.
[20] K. Shmueli, J. Li, J.H. Duyn, Magnetic susceptibility mapping of brain tissue in-vivo using MRI phase data, Magn. Reson. Med. 62 (2009) 1510–1522.
[21] L. de Rochefort, T. Liu, B. Kressler, J. Liu, P. Spincemaille, V. Lebon, J. Wu, Y. Wang, Quantitative susceptibility map reconstruction from MR phase data using bayesian regularization: validation and application to brain imaging, Magn. Reson. Med. 63 (2010) 194–206.
[22] F. Schweser, A. Deistung, B.W. Lehr, J.R. Reichenbach, Quantitative imaging of intrinsic magnetic tissue properties using MRI signal phase: an approach to in vivo brain iron metabolism?, Neuroimage 54 (2011) 2789–2807
[23] C.J. Wiggins, V. Gudmundsdottir, D. Le Bihan, V. Lebon, M. Chaumeil, Orientation dependence of white matter T_2^* contrast at 7 T: a direct demonstration, Proc. Soc. Magn. Magn. Reson. Med. (2008) 237.
[24] J. Lee, K. Shmueli, M. Fukunaga, P. van Gelderen, H. Merkle, A.C. Silva, J.H. Duyn, Sensitivity of MRI resonance frequency to the orientation of brain tissue microstructure, Proc. Natl. Acad. Sci. USA 107 (2010) 5130–5135.
[25] C. Liu, Susceptibility tensor imaging, Magn. Reson. Med. 63 (2010) 1471–1477.
[26] P. Sati, P. van Gelderen, A.C. Silva, D.S. Reich, H. Merkle, J. de Zwart, J.H. Duyn, The magnetic microstructure of cerebral white matter, Neuroimage, submitted for publication.
[27] J.F. Schenck, The role of magnetic susceptibility in magnetic resonance imaging: MRI magnetic compatibility of the first and second kinds, Med. Phys. 23 (1996) 815–850.
[28] W.A. Edelstein, J.M. Hutchison, G. Johnson, T. Redpath, Spin warp NMR imaging and applications to human whole-body imaging, Phys. Med. Biol. 25 (1980) 751–756.
[29] D.A. Yablonskiy, E.M. Haacke, Theory of NMR signal behavior in magnetically inhomogeneous tissues: the static dephasing regime, Magn. Reson. Med. 32 (1994) 749–763.
[30] A.L. Sukstanskii, D.A. Yablonskiy, Gaussian approximation in the theory of MR signal formation in the presence of structure-specific magnetic field inhomogeneities. Effects of impermeable susceptibility inclusions, J. Magn. Reson. 167 (2004) 56–67.
[31] Y.P. Du, R. Chu, D. Hwang, M.S. Brown, B.K. Kleinschmidt-DeMasters, D. Singel, J.H. Simon, Fast multislice mapping of the myelin water fraction using multicompartment analysis of T_2^* decay at 3 T: a preliminary postmortem study, Magn. Reson. Med. 58 (2007) 865–870.
[32] P. van Gelderen, J.A. de Zwart, J. Lee, P. Sati, D.S. Reich, J.H. Duyn, Nonexponential T(2) decay in white matter, Magn. Reson. Med. 67 (2012) 110–117.
[33] Y. Xu, J.A. Balschi, C.S. Springer Jr., Magnetic susceptibility shift selected imaging: MESSI, Magn. Reson. Med. 16 (1990) 80–90.
[34] W. Du, Y.P. Du, U. Bick, X. Fan, P.M. MacEneaney, M.A. Zamora, M. Medved, G.S. Karczmar, Breast MR imaging with high spectral and spatial resolutions: preliminary experience, Radiology 224 (2002) 577–585.

[35] V. Sehgal, Z. Delproposto, E.M. Haacke, K.A. Tong, N. Wycliffe, D.K. Kido, Y. Xu, J. Neelavalli, D. Haddar, J.R. Reichenbach, Clinical applications of neuroimaging with susceptibility-weighted imaging, J. Magn. Reson. Imaging: JMRI 22 (2005) 439–450.

[36] B. Yao, T.Q. Li, P. Gelderen, K. Shmueli, J.A. de Zwart, J.H. Duyn, Susceptibility contrast in high field MRI of human brain as a function of tissue iron content, Neuroimage 44 (2009) 1259–1266.

[37] D.B. Kell, Towards a unifying, systems biology understanding of large-scale cellular death and destruction caused by poorly liganded iron: Parkinson's, Huntington's, Alzheimer's, prions, bactericides, chemical toxicology and others as examples, Arch. Toxicol. 84 (2010) 825–889.

[38] D.B. Kell, Iron behaving badly: inappropriate iron chelation as a major contributor to the aetiology of vascular and other progressive inflammatory and degenerative diseases, BMC Med. Genomics 2 (2009) 2.

[39] R.P. Kennan, J. Zhong, J.C. Gore, Intravascular susceptibility contrast mechanisms in tissues, Magn. Reson. Med. 31 (1994) 9–21.

[40] J.L. Boxerman, L.M. Hamberg, B.R. Rosen, R.M. Weisskoff, MR contrast due to intravascular magnetic susceptibility perturbations, Magn. Reson. Med. 34 (1995) 555–566.

[41] J. Sedlacik, A. Rauscher, J.R. Reichenbach, Obtaining blood oxygenation levels from MR signal behavior in the presence of single venous vessels, Magn. Reson. Med. 58 (2007) 1035–1044.

[42] A.P. Fan, T. Benner, D.S. Bolar, B.R. Rosen, E. Adalsteinsson, Phase-based regional oxygen metabolism (PROM) using MRI, Magn. Reson. Med. 67 (2012) 669–678.

[43] V. Jain, M.C. Langham, F.W. Wehrli, MRI estimation of global brain oxygen consumption rate, J. Cerebr. Blood Flow Metab. 30 (2010) 1598–1607.

[44] S.A. Gronemeyer, J.W. Langston, S.L. Hanna, J.W. Langston Jr., MR imaging detection of calcified intracranial lesions and differentiation from iron-laden lesions, J. Magn. Reson. Imaging: JMRI 2 (1992) 271–276.

[45] N. Yamada, S. Imakita, T. Sakuma, M. Takamiya, Intracranial calcification on gradient-echo phase image: depiction of diamagnetic susceptibility, Radiology 198 (1996) 171–178.

[46] R.J. Ogg, J.W. Langston, E.M. Haacke, R.G. Steen, J.S. Taylor, The correlation between phase shifts in gradient-echo MR images and regional brain iron concentration, Magn. Reson. Imaging 17 (1999) 1141–1148.

[47] S. Wharton, R. Bowtell, Whole-brain susceptibility mapping at high field: a comparison of multiple- and single-orientation methods, Neuroimage 53 (2010) 515–525.

[48] B. Wu, W. Li, A. Guidon, C. Liu, Whole brain susceptibility mapping using compressed sensing, Magn. Reson. Med. 67 (2012) 137–147.

[49] J. Liu, T. Liu, L. de Rochefort, J. Ledoux, I. Khalidov, W. Chen, A.J. Tsiouris, C. Wisnieff, P. Spincemaille, M.R. Prince, Y. Wang, Morphology enabled dipole inversion for quantitative susceptibility mapping using structural consistency between the magnitude image and the susceptibility map, Neuroimage 59 (2012) 2560–2568.

[50] F. Schweser, K. Sommer, A. Deistung, J.R. Reichenbach, Quantitative susceptibility mapping for investigating subtle susceptibility variations in the human brain, Neuroimage 62 (2012) 2083–2100.

[51] G. Deville, M. Bernier, J.M. Delrieux, NMR multiple echoes observed in solid He-3, Phys. Rev. B 19 (1979) 5666–5688.

[52] R. Salomir, B.D. de Senneville, C.T.W. Moonen, A fast calculation method for magnetic field inhomogeneity due to an arbitrary distribution of bulk susceptibility, Concepts Magn. Reson. B 19B (2003) 26–34.

[53] S. Wharton, A. Schafer, R. Bowtell, Susceptibility mapping in the human brain using threshold-based k-space division, Magn. Reson. Med. 63 (2010) 1292–1304.

[54] T. Liu, P. Spincemaille, L. de Rochefort, B. Kressler, Y. Wang, Calculation of susceptibility through multiple orientation sampling (COSMOS): a method for conditioning the inverse problem from measured magnetic field map to susceptibility source image in MRI, Magn. Reson. Med. 61 (2009) 196–204.

[55] T. Liu, J. Liu, L. de Rochefort, P. Spincemaille, I. Khalidov, J.R. Ledoux, Y. Wang, Morphology enabled dipole inversion (MEDI) from a single-angle acquisition: comparison with COSMOS in human brain imaging, Magn. Reson. Med. 66 (2011) 777–783.

[56] G.A. Christoforidis, E.C. Bourekas, M. Baujan, A.M. Abduljalil, A. Kangarlu, D.G. Spigos, D.W. Chakeres, P.M. Robitaille, High resolution MRI of the deep brain vascular anatomy at 8 Tesla: susceptibility-based enhancement of the venous structures, J. Comput. Assist. Tomogr. 23 (1999) 857–866.

[57] X. He, M. Zhu, D.A. Yablonskiy, Validation of oxygen extraction fraction measurement by qBOLD technique, Magn. Reson. Med. 60 (2008) 882–888.

[58] B. Drayer, P. Burger, R. Darwin, S. Riederer, R. Herfkens, G.A. Johnson, MRI of brain iron, AJR Am. J. Roentgenol. 147 (1986) 103–110.

[59] R.J. Ordidge, J.M. Gorell, J.C. Deniau, R.A. Knight, J.A. Helpern, Assessment of relative brain iron concentrations using T2-weighted and T_2^*-weighted MRI at 3 Tesla, Magn. Reson. Med. 32 (1994) 335–341.

[60] M. Fukunaga, T.Q. Li, P. van Gelderen, J.A. de Zwart, K. Shmueli, B. Yao, J. Lee, D. Maric, M.A. Aronova, G.F. Zhang, R.D. Leapman, J.F. Schenck, H. Merkle, J.H. Duyn, Layer-specific variation of iron content in cerebral cortex as a source of MRI contrast, Proc. Natl. Acad. Sci. USA 107 (2010) 3834–3839.

[61] J. Lee, Y. Hirano, M. Fukunaga, A.C. Silva, J.H. Duyn, On the contribution of deoxy-hemoglobin to MRI gray–white matter phase contrast at high field, Neuroimage 49 (2010) 193–198.

[62] B. Weber, A.L. Keller, J. Reichold, N.K. Logothetis, The microvascular system of the striate and extrastriate visual cortex of the macaque, Cereb. Cortex 18 (2008) 2318–2330.

[63] J.R. Reichenbach, R. Venkatesan, D.A. Yablonskiy, M.R. Thompson, S. Lai, E.M. Haacke, Theory and application of static field inhomogeneity effects in gradient-echo imaging, J. Magn. Reson. Imaging: JMRI 7 (1997) 266–279.

[64] B. Hallgren, P. Sourander, The effect of age on the non-haemin iron in the human brain, J. Neurochem. 3 (1958) 41–51.

[65] C. Liu, W. Li, G.A. Johnson, B. Wu, High-field (9.4 T) MRI of brain dysmyelination by quantitative mapping of magnetic susceptibility, Neuroimage 56 (2011) 930–938.

[66] J. Lee, K. Shmueli, B.T. Kang, B. Yao, M. Fukunaga, P. van Gelderen, S. Palumbo, F. Bosetti, A.C. Silva, J.H. Duyn, The contribution of myelin to magnetic susceptibility-weighted contrasts in high-field MRI of the brain, Neuroimage 59 (2012) 3967–3975.

[67] C. Langkammer, F. Schweser, N. Krebs, A. Deistung, W. Goessler, E. Scheurer, K. Sommer, G. Reishofer, K. Yen, F. Fazekas, S. Ropele, J.R. Reichenbach, Quantitative susceptibility mapping (QSM) as a means to measure brain iron? A post mortem validation study, Neuroimage (2012).

[68] G.A. Lodygensky, J.P. Marques, R. Maddage, E. Perroud, S.V. Sizonenko, P.S. Huppi, R. Gruetter, In vivo assessment of myelination by phase imaging at high magnetic field, Neuroimage 59 (2012) 1979–1987.

[69] T.Q. Li, B. Yao, P. van Gelderen, H. Merkle, S. Dodd, L. Talagala, A.P. Koretsky, J. Duyn, Characterization of T(2)(star) heterogeneity in human brain white matter, Magn. Reson. Med. 62 (2009) 1652–1657.

[70] J.T. Curnes, P.C. Burger, W.T. Djang, O.B. Boyko, MR imaging of compact white matter pathways, AJNR Am. J. Neuroradiol. 9 (1988) 1061–1068.

[71] A. Cherubini, P. Peran, G.E. Hagberg, A.E. Varsi, G. Luccichenti, C. Caltagirone, U. Sabatini, G. Spalletta, Characterization of white matter fiber bundles with T_2^* relaxometry and diffusion tensor imaging, Magn. Reson. Med. 61 (2009) 1066–1072.

[72] B. Bender, U. Klose, The in vivo influence of white matter fiber orientation towards B(0) on T_2^* in the human brain, NMR Biomed. 23 (2010) 1071–1076.

[73] C. Denk, E. Hernandez Torres, A. MacKay, A. Rauscher, The influence of white matter fibre orientation on MR signal phase and decay, NMR Biomed. 24 (2011) 246–252.

[74] J. Lee, P. van Gelderen, L.W. Kuo, H. Merkle, A.C. Silva, J.H. Duyn, T_2^*-based fiber orientation mapping, Neuroimage 57 (2011) 225–234.

[75] S. Kohler, K.H. Hiller, C. Waller, W.R. Bauer, A. Haase, P.M. Jakob, Investigation of the microstructure of the isolated rat heart: a comparison between T_2^*- and diffusion-weighted MRI, Magn. Reson. Med. 50 (2003) 1144–1150.

[76] P. Sati, A.C. Silva, P. van Gelderen, M.I. Gaitan, J.E. Wohler, S. Jacobson, J.H. Duyn, D.S. Reich, In vivo quantification of T(2) anisotropy in white matter fibers in marmoset monkeys, Neuroimage 59 (2012) 979–985.

[77] X. He, D.A. Yablonskiy, Biophysical mechanisms of phase contrast in gradient echo MRI, Proc. Natl. Acad. Sci. USA 106 (2009) 13558–13563.

[78] S.C. Chu, Y. Xu, J.A. Balschi, C.S. Springer Jr., Bulk magnetic susceptibility shifts in NMR studies of compartmentalized samples: use of paramagnetic reagents, Magn. Reson. Med. 13 (1990) 239–262.

[79] C. Boesch, J. Slotboom, H. Hoppeler, R. Kreis, In vivo determination of intra-myocellular lipids in human muscle by means of localized 1H-MR-spectroscopy, Magn. Reson. Med. 37 (1997) 484–493.

[80] D.L. Worcester, Structural origins of diamagnetic anisotropy in proteins, Proc. Natl. Acad. Sci. USA 75 (1978) 5475–5477.

[81] E. Boroske, W. Helfrich, Magnetic anisotropy of egg lecithin membranes, Biophys. J . 24 (1978) 863–868.

[82] F.T. Hong, D. Mauzerall, A. Mauro, Magnetic anisotropy and the orientation of retinal rods in a homogeneous magnetic field, Proc. Natl. Acad. Sci. USA 68 (1971) 1283–1285.

[83] W. Arnold, R. Steele, H. Mueller, On the magnetic asymmetry of muscle fibers, Proc. Natl. Acad. Sci. USA 44 (1958) 1–4.

[84] X. Li, D.S. Vikram, I.A. Lim, C.K. Jones, J.A. Farrell, P.C. van Zijl, Mapping magnetic susceptibility anisotropies of white matter in vivo in the human brain at 7 T, Neuroimage 62 (2012) 314–330.

[85] E.F. Soto, L. Seminario de Bohner, M. Del Carmen Calvino, Chemical composition of myelin and other subcellular fractions isolated from bovine white matter, J. Neurochem. 13 (1966) 989–998.

[86] J.S. O'Brien, E.L. Sampson, Lipid composition of the normal human brain: gray matter, white matter, and myelin, J. Lipid Res. 6 (1965) 537–544.

[87] K. Lonsdale, Diamagnetic anisotropy of organic molecules, Proc. R. Soc. London, Ser. A 171 (1939) 0541–0568.

[88] W. Li, B. Wu, A.V. Avram, C. Liu, Magnetic susceptibility anisotropy of human brain in vivo and its molecular underpinnings, Neuroimage 59 (2012) 2088–2097.

[89] A. MacKay, C. Laule, I. Vavasour, T. Bjarnason, S. Kolind, B. Madler, Insights into brain microstructure from the T2 distribution, Magn. Reson. Imaging 24 (2006) 515–525.

[90] K.D. Harkins, A.N. Dula, M.D. Does, Effect of intercompartmental water exchange on the apparent myelin water fraction in multiexponential T2 measurements of rat spinal cord, Magn. Reson. Med. 67 (2012) 793–800.

[91] K. Wachowicz, R.E. Snyder, Assignment of the T(2) components of amphibian peripheral nerve to their microanatomical compartments, Magn. Reson. Med. 47 (2002) 239–245.

[92] I.M. Vavasour, K.P. Whittall, A.L. MacKay, D.K. Li, G. Vorobeychik, D.W. Paty, A comparison between magnetization transfer ratios and myelin water percentages in normals and multiple sclerosis patients, Magn. Reson. Med. 40 (1998) 763–768.

[93] C. Laule, I.M. Vavasour, G.R. Moore, J. Oger, D.K. Li, D.W. Paty, A.L. MacKay, Water content and myelin water fraction in multiple sclerosis. A *T*2 relaxation study, J. Neurol. 251 (2004) 284–293.

[94] C. Lenz, M. Klarhofer, K. Scheffler, Limitations of rapid myelin water quantification using 3D bSSFP, Magma 23 (2010) 139–151.

[95] J. Dennie, J.B. Mandeville, J.L. Boxerman, S.D. Packard, B.R. Rosen, R.M. Weisskoff, NMR imaging of changes in vascular morphology due to tumor angiogenesis, Magn. Reson. Med. 40 (1998) 793–799.

[96] J.H. Duyn, A.P. Koretsky, Novel frontiers in ultra-structural and molecular MRI of the brain, Curr. Opin. Neurol. 24 (2011) 386–393.

[97] G. Zabow, S. Dodd, J. Moreland, A. Koretsky, Micro-engineered local field control for high-sensitivity multispectral MRI, Nature 453 (2008) 1058–1063.

[98] G. Zabow, S.J. Dodd, E. Shapiro, J. Moreland, A.P. Koretsky, Microfabricated high-moment micrometer-sized MRI contrast agents, Magn. Reson. Med. 65 (2011) 645–655.

[99] C. Liu, W. Li, B. Wu, Y. Jiang, G.A. Johnson, 3D fiber tractography with susceptibility tensor imaging, Neuroimage 59 (2012) 1290–1298.

[100] M. Matsumae, D. Kurita, H. Atsumi, M. Haida, O. Sato, R. Tsugane, Sequential changes in MR water proton relaxation time detect the process of rat brain myelination during maturation, Mech. Ageing Dev. 122 (2001) 1281–1291.

[101] A. Vignaud, I. Rodriguez, D.B. Ennis, R. DeSilva, P. Kellman, J. Taylor, E. Bennett, H. Wen, Detection of myocardial capillary orientation with intravascular iron-oxide nanoparticles in spin-echo MRI, Magn. Reson. Med. 55 (2006) 725–730.

[102] C. Boesch, R. Kreis, Dipolar coupling and ordering effects observed in magnetic resonance spectra of skeletal muscle, NMR Biomed. 14 (2001) 140–148.

[103] G.D. Fullerton, I.L. Cameron, V.A. Ord, Orientation of tendons in the magnetic field and its effect on T2 relaxation times, Radiology 155 (1985) 433–435.

[104] W. Grunder, M. Kanowski, M. Wagner, A. Werner, Visualization of pressure distribution within loaded joint cartilage by application of angle-sensitive NMR microscopy, Magn. Reson. Med. 43 (2000) 884–891.

[105] R.M. Henkelman, G.J. Stanisz, J.K. Kim, M.J. Bronskill, Anisotropy of NMR properties of tissues, Magn. Reson. Med. 32 (1994) 592–601.

[106] J.R. Connor, S.L. Menzies, S.M. St Martin, E.J. Mufson, Cellular distribution of transferrin, ferritin, and iron in normal and aged human brains, J. Neurosci. Res. 27 (1990) 595–611.

[107] T.A. Rouault, Iron on the brain, Nat. Genet. 28 (2001) 299–300.

[108] J. Budde, G. Shajan, J. Hoffmann, K. Ugurbil, R. Pohmann, Human imaging at 9.4 T using T_2^*-, phase-, and susceptibility-weighted contrast, Magn. Reson. Med. 65 (2011) 544–550.

[109] J.H. Duyn, The future of ultra-high field MRI and fMRI for study of the human brain, Neuroimage 62 (2012) 1241–1248.